Electronic Supplementary Material (ESI) for Journal of Materials Chemistry A.

Supporting Information for

Yolk–Shell Structured FeS/MoS_2@Nitrogen-Doped Carbon Nanocubes with Sufficient Internal Void Space as an Ultrastable Anodes for Potassium-Ion Batteries

Jianhua Chu,[a] Qiyao Yu,*[b] Kun Han,[a] Lidong Xing,[a] Chao Gu,[a] Ying Li,[b] Yanping Bao,*[a] and Wei (Alex) Wang[c]

[a] *State Key Laboratory of Advanced Metallurgy, University of Science and Technology Beijing, Beijing 100083, China. Email: baoyp@ustb.edu.cn*

[b] *Institute of Advanced Structure Technology, Beijing Institute of Technology, Beijing 100081, China. Email: qiyaoyu@bit.edu.cn*

[c] *Beijing Key Laboratory of Bio-inspired Energy Materials and Devices, School of Space and Environment, Beihang University, Beijing 100191, China*

† Electronic supplementary information (ESI) available. See DOI: xxxxxxxx

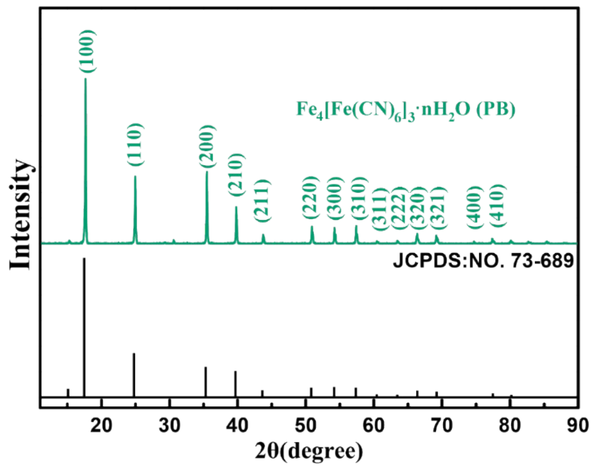

Fig. S1 XRD patterns of Prussian Blue nanocubes.

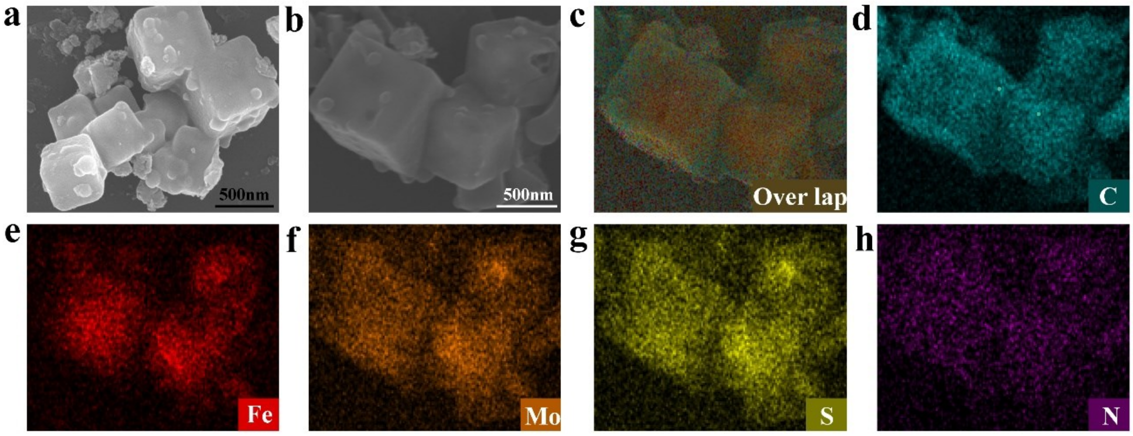

Fig. S2 (a-b) FESEM image and corresponding (c-h) EDS mappings of the as-synthesized FMC.

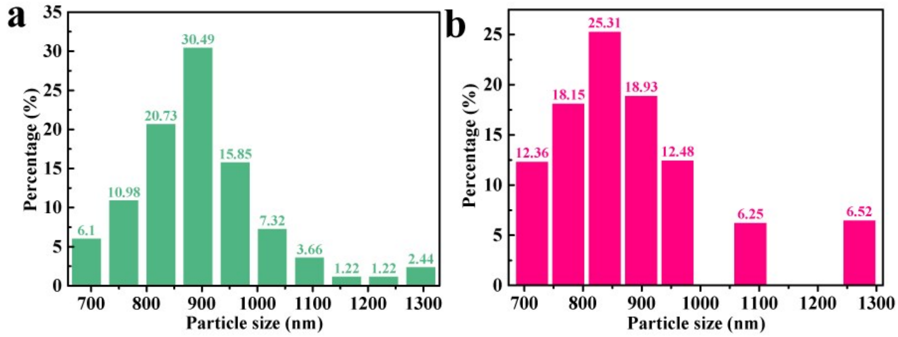

Fig. S3 The size distribution of (a) PB and (b) FMC.

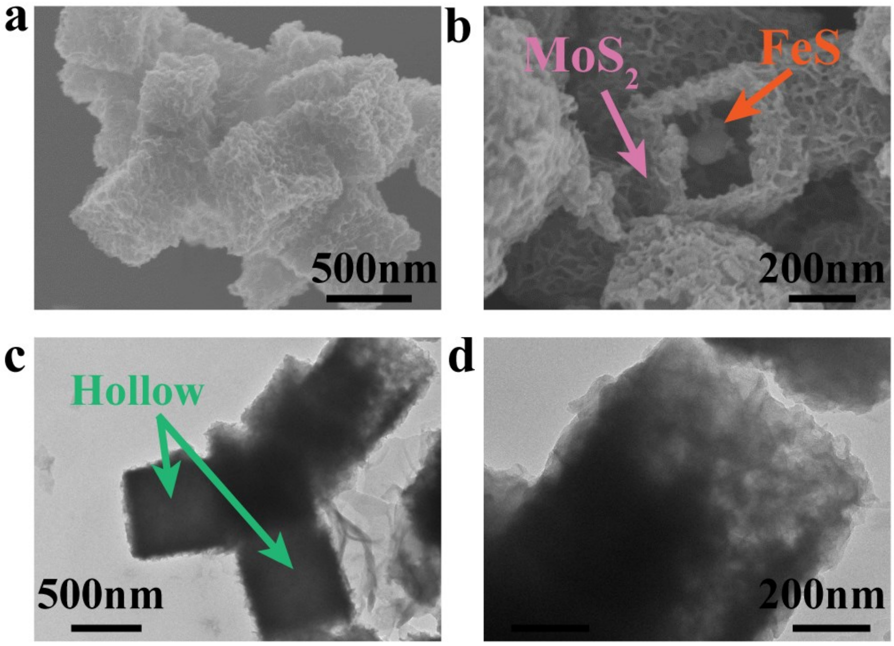

Fig. S4 (a, b) FESEM and (c, d) TEM images of FMCM.

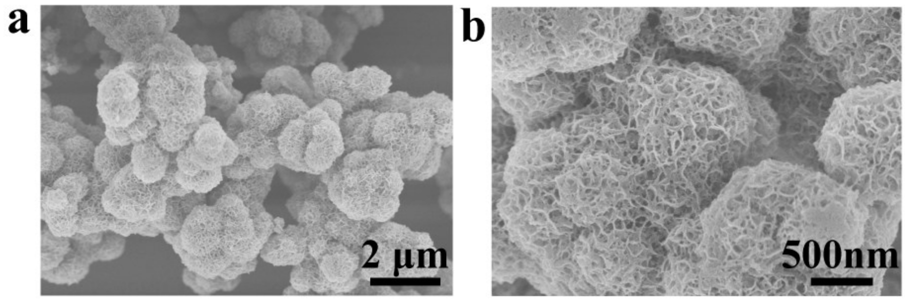

Fig. S5 FESEM images of MS2.

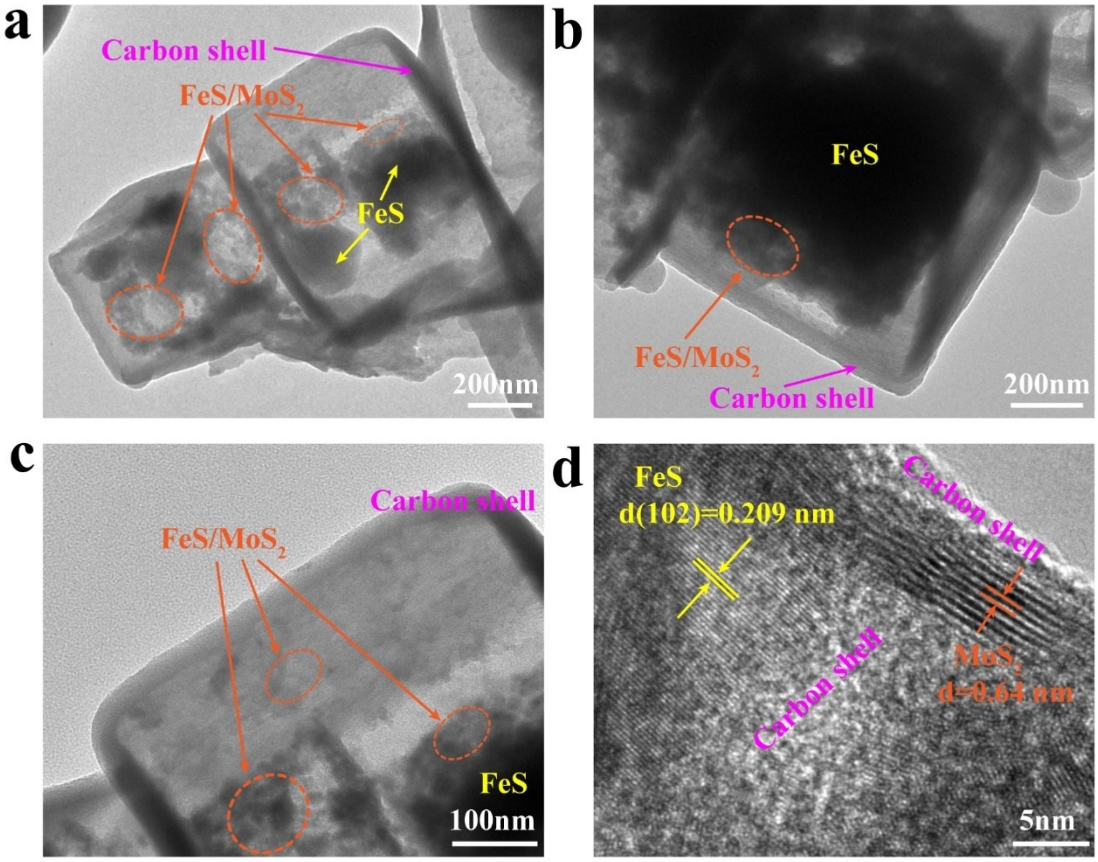

Fig. S6 (a-c) TEM and (d) HRTEM images of the as- synthesized FMC.

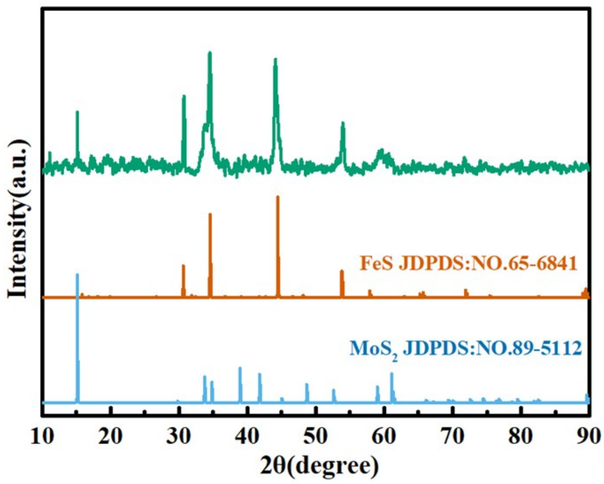

Fig. S7 XRD patterns of FMCM.

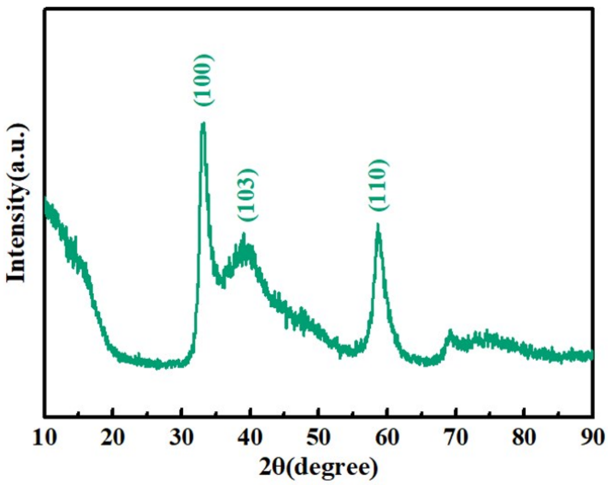

Fig. S8 XRD patterns of MS2.

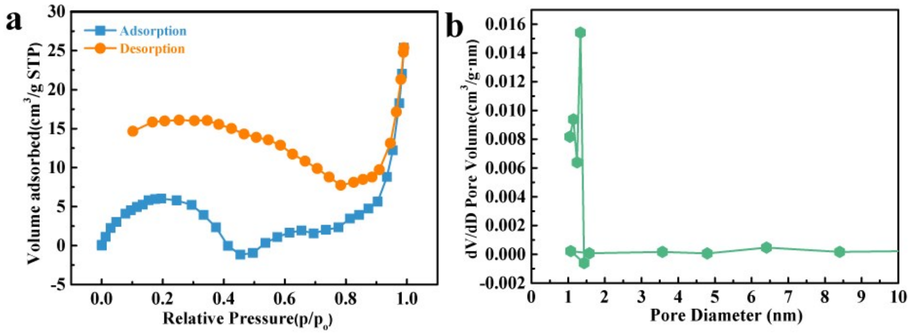

Fig. S9 (a) N_2 adsorption–desorption isotherms and (b) corresponding pore size distribution of FMCM.

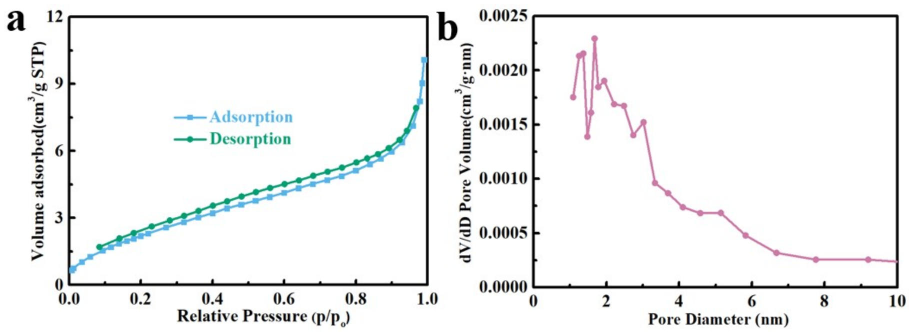

Fig. S10 (a) N_2 adsorption isotherms and (b) corresponding pore size distribution of PB.

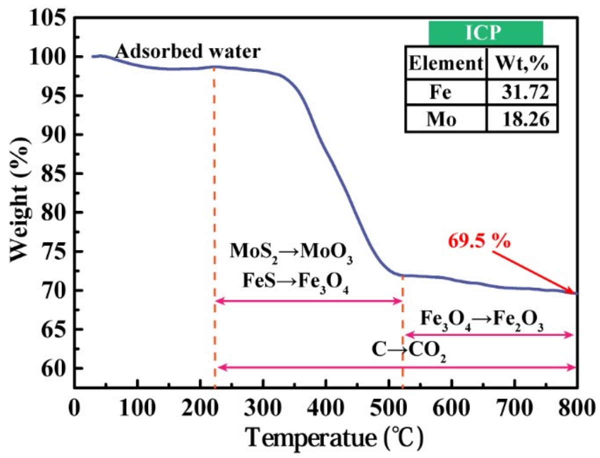

Fig. S11 Thermogravimetric curve of FMC thermally treated in air with a heating rate of 10 °C min^{-1} from room temperature to 800 °C and ICP data of FMC (insert of figure).

Calculation details: The weight loss between 250-550 °C results from the oxidation of MoS_2 and FeS into MoO_3 and Fe_3O_4. The Fe_3O_4 was completely converted into Fe_2O_3 and N-doping carbon shell was completely decomposed when the temperature rises to 800 ℃. Thus, the remaining mass (69.5%) is attributed to stable oxidation states of MoO_3 and Fe_2O_3. According to the results of ICP (insert of Fig. S11), the atomic ratio of Fe and Mo in FMC is 2.98:1. Thus, the 65.7 wt% product includes 42.87 wt% Fe_2O_3 and 26.63 wt% MoO_3 calculated by the following equation.

$$w_{Fe_2O_3} = \frac{\frac{2.98}{2} \times M_{Fe_2O_3}}{\frac{2.98}{2} \times M_{Fe_2O_3} + 1 \times M_{MoO_3}}$$

Further, 42.87 wt% Fe_2O_3 corresponds to 47.16 wt% FeS according to the equation:

$$w_{FeS} = \frac{w_{Fe_2O_3} \times 2M_{FeS}}{M_{Fe_2O_3}}$$

Similarly, 26.63 wt% MoO_3 corresponds to 28.79 wt% FeS. Finally, the content of the carbon component was calculated to be ca. 24.05 wt%.

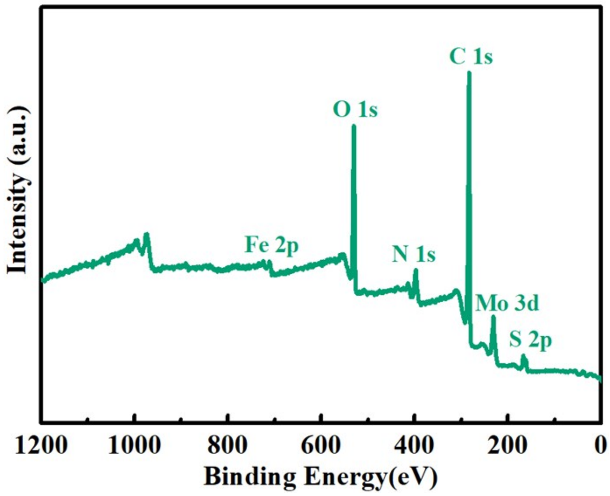

Fig. S12 XPS survey spectrum of the FMC composite.

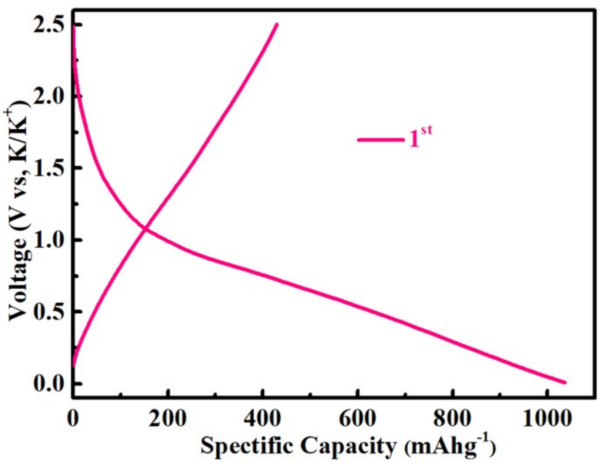

Fig. S13 The initial charge and discharge profiles of FMC composites at 100 mA g^{-1}.

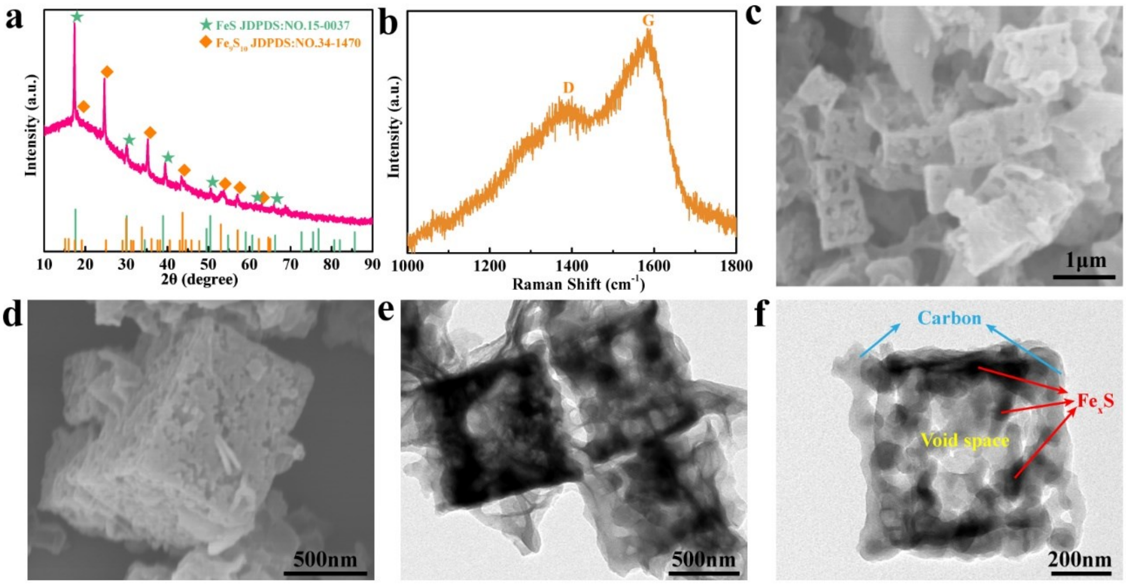

Fig. S14 (a) XRD pattern, (b) Raman spectrum, (c-d) FESEM images and (e-f) TEM images of the as- synthesized Y-S Fe_xS@C.

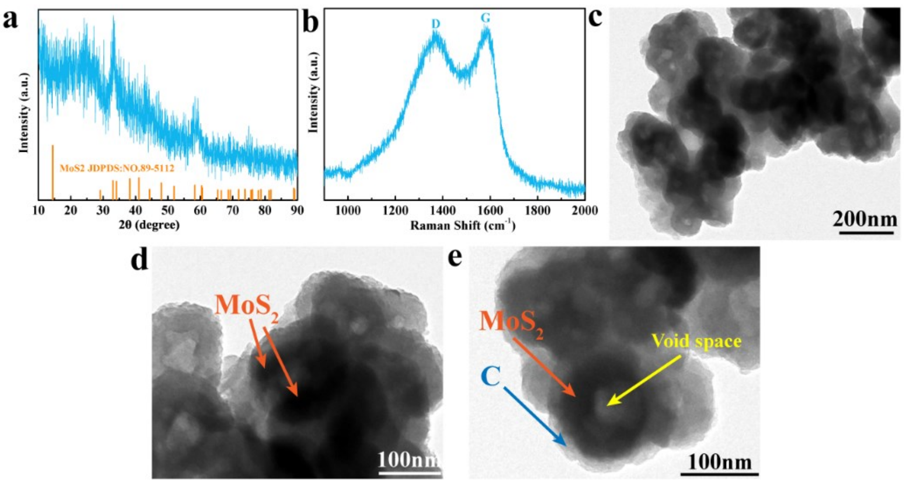

Fig. S15 (a) XRD pattern, (b) Raman spectra and (c-d) TEM images of the as-synthesized Y-S MoS_2@C.

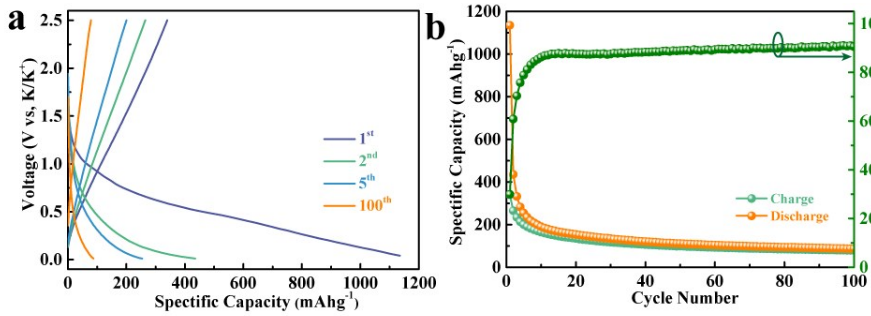

Fig. S16 (a) Charge–discharge voltage profiles from the 1st to 100th cycle and (b) cycle performance of the Y-S $Fe_xS@C$ at 100 mA g^{-1}.

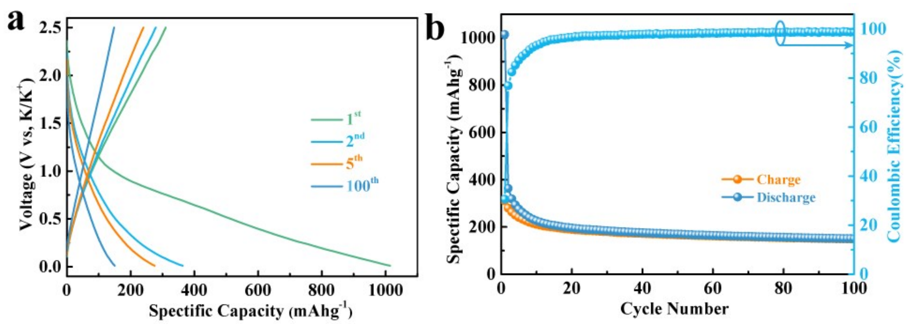

Fig. S17 (a) Charge–discharge voltage profiles from the 1st to 100th cycle and (b) cycle performance of the Y-S MoS_2@C at 100 mA g^{-1}.

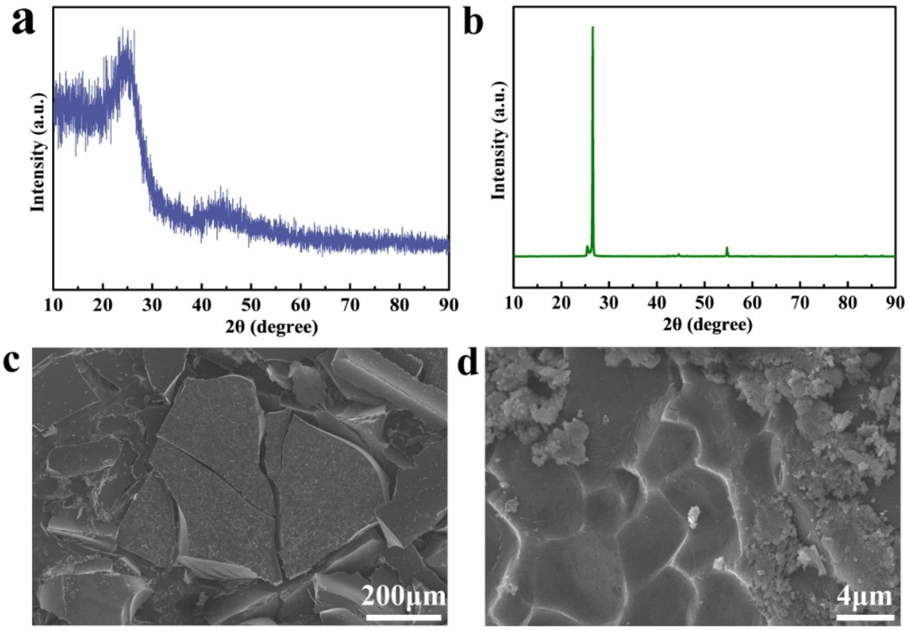

Fig. S18 XRD pattern of (a) N-doped carbon and (b) commercial graphite. (c-d) SEM image of the as- synthesized N-doped carbon.

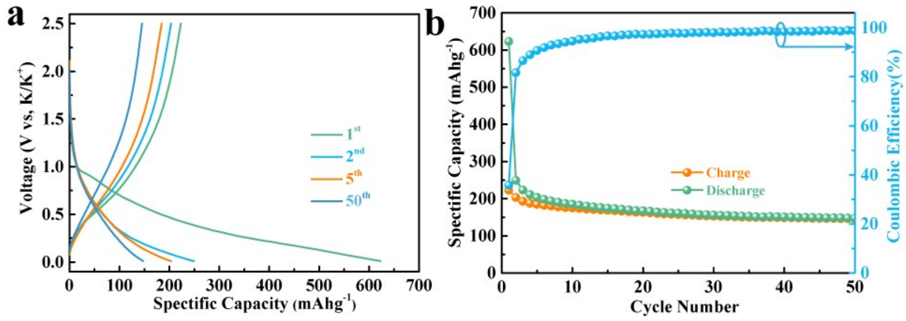

Fig. S19 (a) Charge–discharge voltage profiles from the 1st to 50th cycle and (b) cycle performance of N-doped carbon at 100 mA g^{-1}.

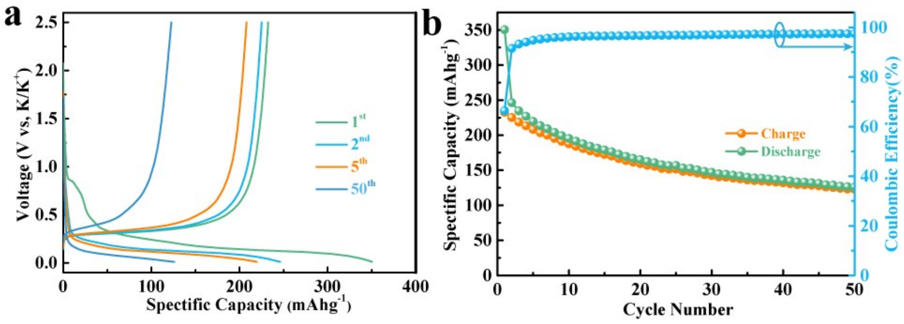

Fig. S20 (a) Charge–discharge voltage profiles from the 1st to 50th cycle and (b) cycle performance of commercial graphite at 100 mA g^{-1}.

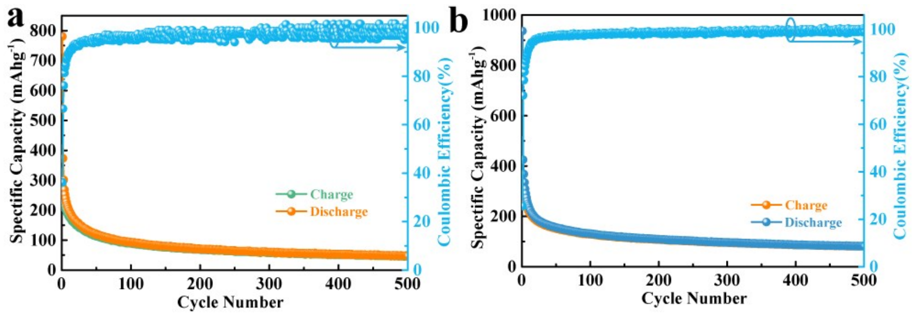

Fig. S21 Long-term cycling performances of the Y-S Fe_xS@C and (g) Y-S MoS_2@C electrodes at a current density of 1000 mA g^{-1}.

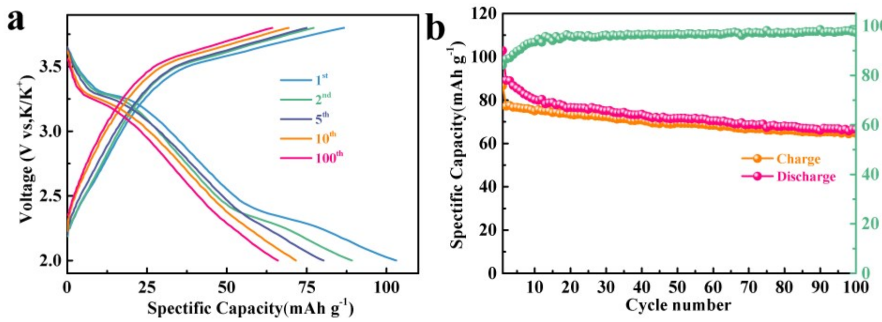

Fig. S22 Electrochemical performance of an FMC// $K_4Fe(CN)_6$ (KPB) K-ion full battery. (a) The 1st, 2nd, 5th, 10th and 100th charge/discharge profiles and (b) cycling performance of the K-ion full battery at 50 mA g^{-1} with the voltage range from 2.0 to 3.8 V.

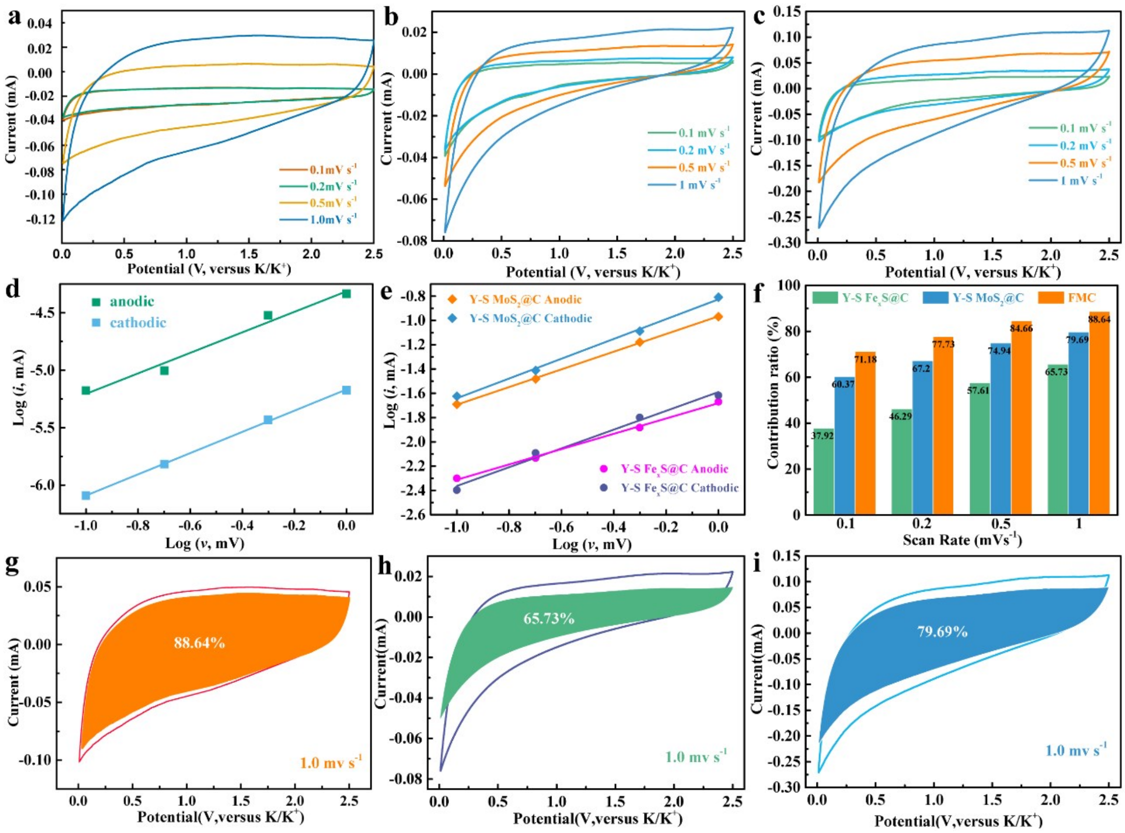

Fig. S23 Analysis of the capacitive behavior for the FMC, Y-S Fe_xS@C and Y-S MoS_2@C electrodes. CV profiles of the (a) FMC, (b) Y-S Fe_xS@C and (c) Y-S MoS_2@C electrodes at different scan rates from 0.1 to 1.0 mV s^{-1} at the voltage window between 0.01 and 2.5 V (*versus* K^+/K). Determination of the b-value according to the relationship between peak current and scan rate for (d) FMC, (e) Y-S Fe_xS@C and Y-S MoS_2@C electrodes, respectively. (f) Contribution ratios of the capacitive and diffusion-controlled capacities at different scan rates for FMC, Y-S Fe_xS@C and Y-S MoS_2@C electrodes. CV curves of the capacitive contribution to the total current at 1 mV s^{-1} for (g) FMC, (h) Y-S Fe_xS@C and (i) Y-S MoS_2@C electrodes.

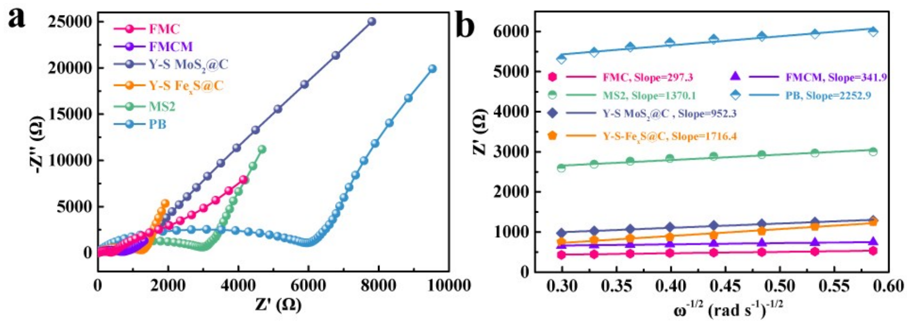

Fig. S24 (a) Nyquist impedance plots and (b) liner relationship between real impedance and reciprocal square root with low frequency for FMC, FMCM, Y-S MoS_2@C, Y-S Fe_xS@C, MS2 and PB electrodes before cycling.

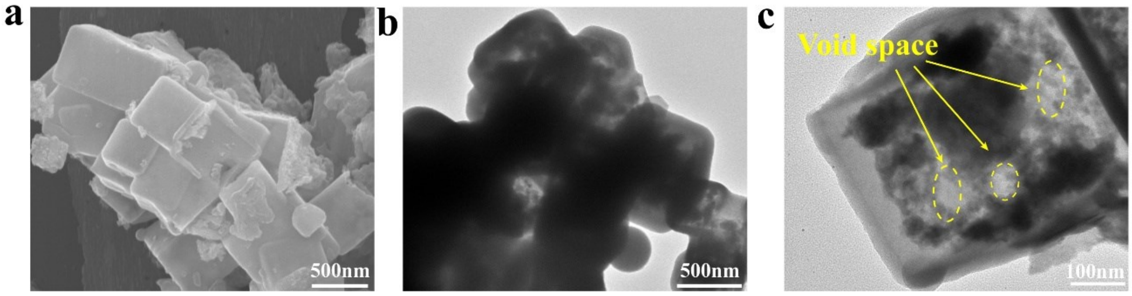

Fig. S25 (a) FESEM and (b-c) TEM images of the FMC electrode after 200 cycles at 200 mA g^{-1}.

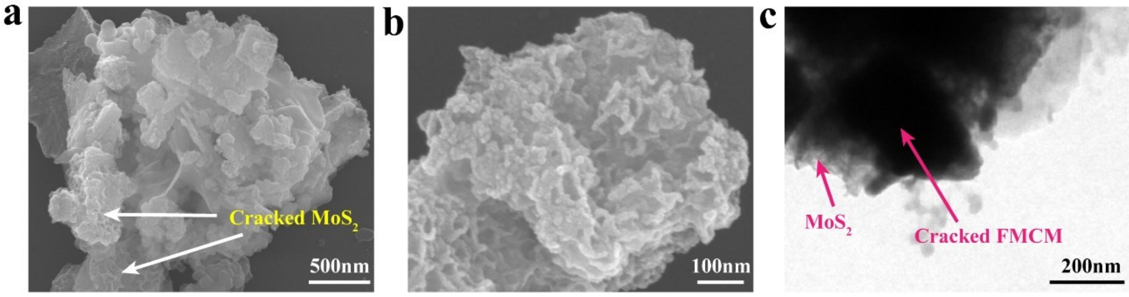

Fig. S26 (a-b) FESEM and (c) TEM images of the FMCM electrode after 200 cycles at 200 mA g^{-1}.

Table S1. Rate performance comparison of some reported carbon-based and sulfides materials anode of KIBs.

Anode materials	Rate	Capacity	Rate	Capacity	Reference
FMC	**50** **200** **1000**	**407** **328** **281**	**100** **500**	**350** **295**	**This work**
FeP@CNBs	200 1000	156 65	500	101	Ref [S1]
Sn_4P_3@C	100 300 1000	378 292 219	200 500	330 255	Ref [S2]
FeS_2@G@CNF	200 1000	332 171	500	243	Ref [S3]
MoS_2@SnO_2@C	100 500	345 153	200 800	276 86	Ref [S4]
CoP@NPPC	100 500	134 94	200 1000	123 74	Ref [S5]
MoS_2/N-doped-C	200 1000	238 171	500	204	Ref [S6]
Fe_3C@PGC-NGF	100 500	310 226	200 1000	252 195	Ref [S7]
$MoSe_2$/N-C	200 1000	224 195	500	211	Ref [S8]
CoS@CNFs	200 800	167 75	400	104	Ref [S9]

Table S2. Cycling stability comparison of some reported anode materials of KIBs.

Anode materials	Cycling stability	Reference
FMC	**342 mAh g^{-1} for 100 cycles at 100 mA g^{-1}** **289 mAh g^{-1} for 200 cycles at 200 mA g^{-1}** **232 mAh g^{-1} for 10000 cycles at 1000 mA g^{-1}**	**This work**
FeP@CNBs	205 mAh g^{-1} for 100 cycles at 100 mA g^{-1}	Ref [S1]
Sn_4P_3@C	315 mAh g^{-1} for 100 cycles at 20 mA g^{-1} 182 mAh g^{-1} for 800 cycles at 500 mA g^{-1}	Ref [S2]
SnS_2@rGO	204 mAh g^{-1} for 300 cycles at 1000 mA g^{-1}	Ref [S10]
FeS_2@G@CNF	205 mAh g^{-1} for 100 cycles at 200 mA g^{-1} 120 mAh g^{-1} for 680 cycles at 1000 mA g^{-1}	Ref [S3]
G@Y–S FeS_2@C	308 mAh g^{-1} for 100 cycles at 300 mA g^{-1} 162 mAh g^{-1} for 1000 cycles at 1000 mA g^{-1}	Ref [S11]
MoS_2@SnO_2@C	312 mAh g^{-1} for 25 cycles at 50 mA g^{-1} 250 mAh g^{-1} for 20 cycles at 100 mA g^{-1}	Ref [S4]
NiS_2@C@C	303 mAh g^{-1} for 100 cycles at 50 mA g^{-1} 117 mAh g^{-1} for 200 cycles at 500 mA g^{-1}	Ref [S12]
CoP@NPPC	127 mAh g^{-1} after 1000 cycles at 100 mA g^{-1} 114 mAh g^{-1} for 1000 cycles at 500 mA g^{-1}	Ref [S5]
MoS_2/N-doped-C	330 mAh g^{-1} for 50 cycles at 50 mA g^{-1} 248 mAh g^{-1} after 100 cycles at 100 mA g^{-1} 212 mAh g^{-1} for 100 cycles at 200 mA g^{-1} 151 mAh g^{-1} for 1000 cycles at 500 mA g^{-1}	Ref [S6]
$MoSe_2$/C	226 mAh g^{-1} after 1000 cycles at 1000 mA g^{-1}	Ref [S8]

Table S3 Kinetic parameters of FMC, FMCM, Y-S MoS_2@C, Y-S Fe_xS@C, MS2 and PB electrodes.

Sample	σ_w [Ω $s^{-0.5}$]	D_{K+} [cm^2 s^{-1}]
FMC	297.3	8.06×10^{-15}
FMCM	341.9	2.94×10^{-15}
Y-S MoS_2@C	952.3	1.19×10^{-16}
Y-S Fe_xS@C	1078	8.98×10^{-17}
MS2	1370.1	5.79×10^{-17}
PB	2252.9	3.43×10^{-16}

Supplementary References

[1] Yang, F.; Gao, H.; Hao, J.; Zhang, S.; Li, P.; Liu, Y.; Chen, J.; Guo, Z., Yolk–Shell Structured FeP@C Nanoboxes as Advanced Anode Materials for Rechargeable Lithium-/Potassium-Ion Batteries. *Adv. Funct. Mater.* **2019,** *29* (16), 1808291.

[2] Li, D.; Zhang, Y.; Sun, Q.; Zhang, S.; Wang, Z.; Liang, Z.; Si, P.; Ci, L., Hierarchically porous carbon supported Sn_4P_3 as a superior anode material for potassium-ion batteries. *Energy Storage Mater.* **2019,** *23*, 367-374.

[3] Chen, C.; Yang, Y.; Tang, X.; Qiu, R.; Wang, S.; Cao, G.; Zhang, M., Graphene-Encapsulated FeS_2 in Carbon Fibers as High Reversible Anodes for Na(+) /K(+) Batteries in a Wide Temperature Range. *Small* **2019,** *15* (10), e1804740.

[4] Chen, Z.; Yin, D.; Zhang, M., Sandwich-like MoS_2@SnO_2 @C with High Capacity and Stability for Sodium/Potassium Ion Batteries. *Small* **2018,** *14* (17), e1703818.

[5] Bai, J.; Xi, B.; Mao, H.; Lin, Y.; Ma, X.; Feng, J.; Xiong, S., One-Step Construction of N,P-Codoped Porous Carbon Sheets/CoP Hybrids with Enhanced Lithium and Potassium Storage. *Adv. Mater.* **2018,** *30* (35), e1802310.

[6] Jia, B.; Yu, Q.; Zhao, Y.; Qin, M.; Wang, W.; Liu, Z.; Lao, C.-Y.; Liu, Y.; Wu, H.; Zhang, Z.; Qu, X., Bamboo-Like Hollow Tubes with MoS_2/N-Doped-C Interfaces Boost Potassium-Ion Storage. *Adv. Funct. Mater.* **2018,** *28* (40), 1803409.

[7] Han, K.; Liu, Z.; Li, P.; Yu, Q.; Wang, W.; Lao, C.-Y.; He, D.; Zhao, W.; Suo, G.; Guo, H.; Song, L.; Qin, M.; Qu, X., High-throughput fabrication of 3D N-doped graphenic framework coupled with Fe_3C@porous graphite carbon for ultrastable potassium ion storage. *Energy Storage Mater.* **2019,** 22, 185-193.

[8] Ge, J.; Fan, L.; Wang, J.; Zhang, Q.; Liu, Z.; Zhang, E.; Liu, Q.; Yu, X.; Lu, B., $MoSe_2$/N-Doped Carbon as Anodes for Potassium-Ion Batteries. *Adv. Energy Mater.* **2018,** *8* (29), 1801477.

[9] Miao, W.; Zhang, Y.; Li, H.; Zhang, Z.; Li, L.; Yu, Z.; Zhang, W., ZIF-8/ZIF-67-derived 3D amorphous carbon-encapsulated CoS/NCNTs supported on CoS-coated carbon nanofibers as an advanced potassium-ion battery anode. *J. Mater. Chem. A* **2019,** *7* (10), 5504-5512.

[10] Chen, X.; Zhang, H.; Ci, C.; Sun, W.; Wang, Y., Few-Layered Boronic Ester Based Covalent Organic Frameworks/Carbon Nanotube Composites for High-Performance K-Organic Batteries. *ACS Nano* **2019,** *13* (3), 3600-3607.
[11] Zhao, Y.; Zhu, J.; Ong, S. J. H.; Yao, Q.; Shi, X.; Hou, K.; Xu, Z. J.; Guan, L., High-Rate and Ultralong Cycle-Life Potassium Ion Batteries Enabled by In Situ Engineering of Yolk-Shell FeS_2@C Structure on Graphene Matrix. *Adv. Energy Mater.* **2018,** *8* (36), 1802565.
[12] Yang, L.; Hong, W.; Zhang, Y.; Tian, Y.; Gao, X.; Zhu, Y.; Zou, G.; Hou, H.; Ji, X., Hierarchical NiS_2 Modified with Bifunctional Carbon for Enhanced Potassium-Ion Storage. *Adv. Funct. Mater.* **2019,** *29* (50), 1903454.